Probing the mechanism by which the retinal G protein transducin activates its biological effector PDE6

Received for publication, October 22, 2023, and in revised form, November 23, 2023 Published, Papers in Press, December 28, 2023,
https://doi.org/10.1016/j.jbc.2023.105608

Cody Aplin[1] **and Richard A. Cerione**[1,2,*]

From the [1]*Department of Chemistry and Chemical Biology and* [2]*Department of Molecular Medicine Cornell University Ithaca New York USA*

Reviewed by members of the JBC Editorial Board. Edited by Henrik Dohlman

Phototransduction in retinal rods occurs when the G protein coupled photoreceptor rhodopsin triggers the activation of phosphodiesterase 6 PDE6) by GTP-bound alpha subunits of the G protein transducin G T). Recently, we presented a cryo-EM structure for a complex between two GTP-bound recombinant G T subunits and native PDE6, that included a bivalent antibody bound to the C-terminal ends of G T and the inhibitor vardena l occupying the active sites on the PDE and PDEβ subunits. We proposed G T-activated PDE6 by inducing a striking reorientation of the PDEγ subunits away from the catalytic sites. However, questions remained including whether in the absence of the antibody G T binds to PDE6 in a similar manner as observed when the antibody is present, does G T activate PDE6 by enabling the substrate cGMP to access the catalytic sites, and how does the lipid membrane enhance PDE6 activation? Here, we demonstrate that 2:1 G T PDE6 complexes form with either recombinant or retinal G T in the absence of the G T antibody. We show that G T binding is not necessary for cGMP nor competitive inhibitors to access the active sites; instead, occupancy of the substrate binding sites enables G T to bind and reposition the PDE6γ subunits to promote catalytic activity. Moreover, we demonstrate by reconstituting G T-stimulated PDE6 activity in lipid bilayer nanodiscs that the membrane-induced enhancement results from an increase in the apparent binding af nity of G T for PDE6. These ndings provide new insights into how the retinal G protein stimulates rapid catalytic turnover by PDE6 required for dim light vision.

The phototransduction pathway in retinal rod cells is responsible for vision in dim light and represents one of the most highly ampli ed and extraordinarily sensitive signaling systems in biology (1–3). The primary components of this pathway are the G protein–coupled receptor (GPCR) rhodopsin (M_r ∼37 kDa), the heterotrimeric G protein transducin (G T, M_r ∼39 kDa, Gβ1, M_r ∼36 kDa, and Gγ1, M_r ∼7 kDa), and the heterotetrametric cyclic GMP (cGMP) phosphodiesterase-6 (PDE6), the biological effector of transducin. PDE6 consists of two highly similar but not identical subunits (PDE6 and PDE6β, M_r ∼100 kDa), each containing a catalytic site and two domains (GAFa and GAFb) that mediate a negative allosteric regulation by cGMP, together with two smaller (identical) subunits (PDE6γ, M_r ∼10 kDa) that are the binding sites for GTP-bound G T (G T GTP). The phototransduction signaling pathway is initiated upon light absorption by the chromophore *cis*-retinal, which is attached *via* a Schiff base linkage to a lysine residue on the seventh transmembrane helix of opsin, the protein backbone of rhodopsin. The absorption of a single photon by rhodopsin catalyzes multiple cycles of transducin activation. Further ampli cation occurs upon the activation of PDE6 by G T GTP, resulting in hydrolysis of more than 10^3 cGMP molecules per second. The reduction in cGMP levels closes cGMP-gated cation channels in retinal rod membranes, resulting in membrane hyperpolarization that initiates the signal transmitted to the optic nerve.

The regulation of PDE6 by activated transducin is a critical and unique feature of the phototransduction pathway that enables vision in dim light. PDE6 is a 3 ,5 -cyclic nucleotide phosphodiesterase and a member of a superfamily of enzymes that play critical roles in compartmentalizing cyclic nucleotide signaling and regulating many physiological processes (4, 5). The PDE superfamily consists of 11 gene families encoding over 100 distinct isozymes, each with a unique tissue distribution and substrate selectivity pro le, making PDEs attractive drug targets due to the prospect of high tissue selectivity with limited off-target effects. Indeed, given their widespread role in human biology, it is unsurprising that PDEs have been found to play a key role in several human diseases including studying retinal diseases, cardiovascular disease, cancer, metabolic diseases, and neurodegenerative disorders (5–12). While the C-terminal catalytic domain is conserved across all PDEs, most members of the PDE superfamily have an N-terminal regulatory domain, which determines the localization and functional diversity of each isozyme. The PDE6 gene family has three isoforms, each with an N-terminal regulatory domain containing tandem GAF domains. PDE6 is the most catalytically active PDE and is the only family member that has coevolved an autoinhibitory PDE6γ subunit, which enables G-protein–stimulated activation and completely prevents basal activity in the absence of G T. This is a critical feature that ensures an exceedingly high signal-to-noise ratio for the signaling output required for vision in dim light.

* For correspondence: Richard A. Cerione, rac1@cornell.edu.

Probing the mechanism by which transducin activates PDE6

While we and others have probed in some detail the molecular basis by which the GPCR rhodopsin activates its G protein signaling partner transducin, and thus have a good picture of how this key step in phototransduction occurs, less is known from a structural and mechanistic perspective regarding how transducin is able to elicit a striking stimulation of PDE6 catalytic activity. Recently, we described a complex that forms between two GTP-bound recombinant G $_{T}$ subunits and PDE6 as determined by cryo-EM (Fig. 1*A*) (13). Based on its structure, we proposed a mechanism by which GTP-bound G $_{T}$ subunits bind to the PDE6γ subunits of PDE6 and cause a signi cant change in their positioning relative to the PDE6 and PDE6β subunits. This appeared to provide both increased access to their catalytic sites and enabled a reversal of the inhibitory constraints on the enzymatic activity imposed by the GAF domains of PDE6. However, to form a stable complex between two G $_{T}$ subunits per PDE6 molecule, we took advantage of earlier ndings that showed how a bivalent antibody targeting the C-terminal end of G $_{T}$ signi cantly increased its af nity for the effector enzyme (14). It was also necessary to occupy the catalytic sites of the PDE6 and PDE6β subunits with vardena l, a competitive inhibitor of the substrate cGMP. Based on our structural determination of this complex, we proposed a working model for how GTP-bound G $_{T}$ subunits activated PDE6. It involved the combined binding of two G $_{T}$ subunits per PDE6 molecule that worked in tandem to release the PDE6γ subunits from the catalytic sites of PDE6 and PDE6β and to reposition the PDE6γ subunits in a manner that removed the inhibitory constraints on catalytic activity imposed by the GAF domains. One key nding of these studies was that the recombinant G $_{T}$* subunits in the G $_{T}$*–PDE6 complex adopt an upside down conformation relative to the presumed location of the plasma membrane based on post-translational lipid modi cations (PTMs) on the C-terminal helices of the PDE6 and PDE6β subunits, the positioning of G $_{s}$ bound to adenylyl cyclase, and the positioning of G $_{T}$ in the rhodopsin–transducin complex (Fig. 1*B*, PDBs: 6R3Q, 6OY9) (13, 15, 16).

Still, there are many questions regarding this proposed mechanism. They include whether the complex that forms between G $_{T}$ and PDE6 in the absence of a bivalent antibody would be the same or different from that observed when the antibody is coupled to G $_{T.}$ Moreover, is a similar complex

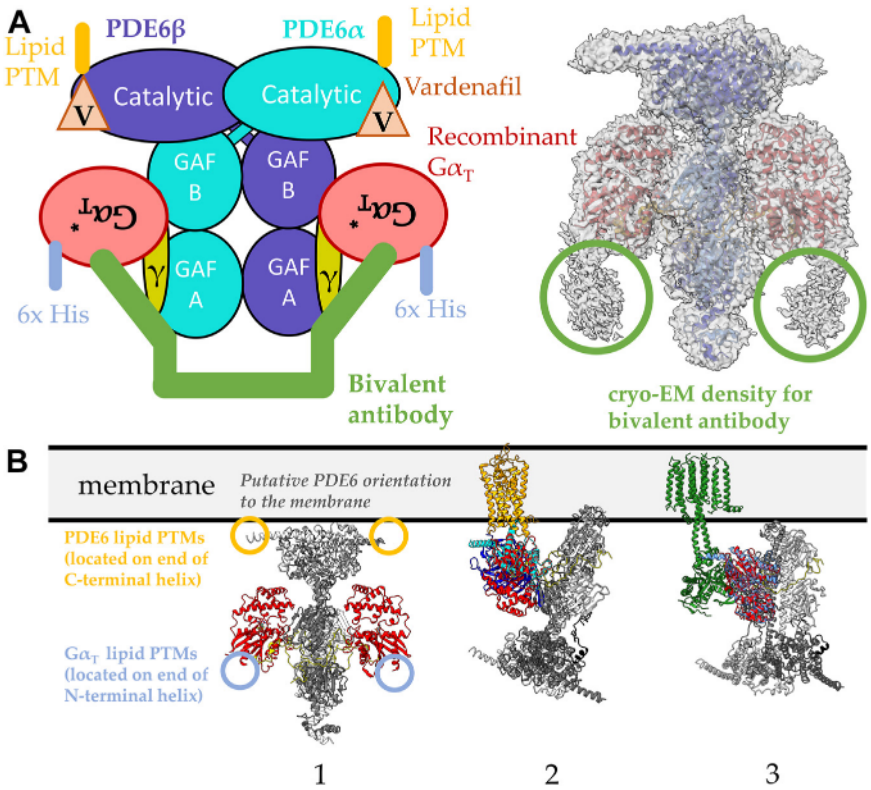

Figure 1. Depictions of the interactions of GTP-bound transducin G subunits with PDE6. *A*, *left:* the cryo-EM structure of the G $_{T}$* PDE6 complex solved by Gao *et al.* was engineered using recombinant G $_{T}$* subunits, a bivalent antibody, and the orthosteric inhibitor vardena l (PDB: 7JSN). *Right:* weak cryo-EM density for the bivalent antibody is observed in the cryo-EM map of G $_{T}$* PDE6 complex (*red circles*, EMDB: 22,458). *B*, comparison of the orientation of the G subunit in different protein complexes. *1*, the presumed association of the 2:1 G $_{T}$ PDE6 complex with the membrane, based on the location of lipid modi cations on the C-terminal helices of the PDE6 and PDE6β subunits (*yellow*). The *upside-down* orientation of G $_{T}$* is highlighted by labeling the location of the N-terminal helix of G $_{T}$*, which contains PTMs in native retinal G $_{T}$ (*blue*). *2*, orientation of the G $_{T}$ subunit in the cryo-EM structure of the rhodopsin transducin complex (PDB: 6OY9) compared to the G $_{T}$ PDE6 complex. One G $_{T}$ subunit is shown in the G $_{T}$ PDE6 complex for simplicity. The structures are aligned by the G $_{T}$ subunits and membrane-bound rhodopsin is used to orient the complexes with the membrane. *3*, orientation of the G $_{s}$ subunit in the cryo-EM structure of adenylyl cyclase bound to G $_{s}$ (PDB: 6R3Q) compared to the G $_{T}$ PDE6 complex. One G $_{T}$ subunit is shown in the G $_{T}$ PDE6 complex for simplicity. The structures are aligned by the G subunits and membrane-bound adenylyl cyclase is used to orient the complexes with the membrane. PDE, phosphodiesterase; PTM, posttranslational lipid modi cation.

assembled when using the native retinal G $_T$ compared to an *Escherichia coli* recombinant, engineered G $_T$ subunit, and what is the mechanistic basis for the observations that a membrane environment as provided by retinal rods signi - cantly enhances the ability of G $_T$ to activate PDE6 (14, 17, 18)? In the studies described below, we have begun to address these questions. We demonstrate that it is possible to form a complex between two recombinant G $_T$ subunits bound to one PDE6 heterotetramer that appears very similar to the complex formed in the presence of a bivalent antibody targeting G $_T$. By determining cryo-EM structures for PDE6 bound to the substrate cGMP as well as to various inhibitors, combined with 3D variability analysis (3DVA) to investigate the effects of substrate/inhibitor binding on the PDE6 holoenzyme, we show how occupancy of the catalytic sites helps to loosen their hold on the PDE6γ subunits and enable activated G $_T$ subunits to reposition them, giving rise to a striking stimulation of enzymatic activity. We present structures of PDE6 bound to either one or two retinal G $_T$ subunits in the presence of the pan-phosphodiesterase inhibitor 3-isobutyl 1-methylxanthine (IBMX). Finally, using lipid nanodiscs as a membrane mimetic system, we show that the membrane-promoted enhancement of PDE6 activation by G $_T$ is tightly controlled through the association of G $_T$ with the membrane and appears to be an outcome of an enhanced af nity of G $_T$ for the effector enzyme.

Results

Examining the ability of G $_T$ to form a complex with PDE6 in the absence of a bivalent antibody

The rst high-resolution structure for a G $_T$–PDE6 complex determined by Gao *et al* (13) was facilitated by stabilization of the complex with an antibody targeting the C-terminal end of G $_T$, together with vardena l, a competitive inhibitor of the substrate cGMP. Here, we set out to determine whether a complex could form between an activated G $_T$ subunit and PDE6 for structural analysis in the absence of a bivalent antibody and vardena l. The samples were prepared by preincubating puri ed native bovine rod PDE6 with a constitutively active recombinant G $_T$ subunit (designated G $_T$*), which was generated by introducing 18 residues from G $_i$ into G $_T$ to facilitate expression in *E coli* and to achieve PDE6 activation, together with two additional mutations (R174C and Q200L) that prevented GTP hydrolysis. After incubating G $_T$* and PDE6 together for 10 min, vardena l was added to each sample and briefly incubated at room temperature before being applied to the cryo-EM grid. All cryo-EM data acquisition, model statistics, and validation is summarized in Tables 1 and 2. Comparison of the 2D classi cation images obtained in previous cryo-EM studies of PDE6 to the images generated in this study shows that in the absence of vardena l, the G $_T$*–PDE6 complex is not stably formed. However, upon the addition of vardena l, the complex forms robustly and the 2D class averages display well-de ned structural features with a stoichiometry of two G $_T$* subunits bound per one PDE6 heterotetramer (Fig. 2*A*).

High-resolution 3D reconstruction of the antibody-free complex was hindered by a preferred orientation. Map quality was assessed using both gold-standard Fourier shell correlation (FSC) analysis as well as 3DFSC (19, 20) for evaluating the directional resolution in the presence of a preferred orientation resulting in map anisotropy. The reported reconstruction resolution was 4.43 Å using the gold-standard FSC resolution (FSC cut-off = 0.143); however, 3DFSC reports a sphericity of 0.830 and a global resolution of 3.3 Å due to missing orientational views in the z-direction (Fig. S1). Despite this, the map displays cryo-EM density for two G $_T$* subunits, allowing for a clear determination of the stoichiometry of the complex (Fig. S1*A*). These results indicate that the ability of activated G $_T$* to form a stable complex with PDE6 requires occupancy of the substrate-binding sites, in this case by a competitive inhibitor. They also show that the induction of a signi cant repositioning of the PDE6γ subunits by G $_T$* along the PDE6 /PDE6β core is not a unique consequence of the bivalent antibody but rather is a natural outcome of the binding of activated G $_T$* to PDE6.

Examining the relationship between G $_T$ binding to PDE6 and occupancy of its catalytic site by a competitive inhibitor of cGMP

We previously assumed that a key role for activated G $_T$ in stimulating PDE6 activity involved its ability to alter the positioning of the PDE6γ subunits relative to the active sites on PDE6 and PDE6β, thus enabling the substrate cGMP to bind and undergo catalytic turnover. However, because we nd that the binding of the competitive inhibitor vardena l to the catalytic sites of PDE6 is necessary to form a complex between activated G $_T$ and PDE6, it appears that the reverse is in fact true, that is, occupancy of the enzyme active sites is necessary for a G $_T$ subunit to bind PDE6. We examined this possibility further using the vardena l analog udena l. To see how this inhibitor affects the structural features of PDE6, we rst determined a high-resolution reconstruction of the cryo-EM structure for the PDE6 holoenzyme alone (Table 1). The resulting 3.1 Å cryo-EM map shows that the overall structure of the PDE6 heterotetramer is in good agreement with the cryo-EM structure of the PDE6 holoenzyme determined by Gulati *et al* (PDB: 6MZB, EMDB: 9297) (21) with an overall RMSD of 1 Å, although the resolution was improved from 3.4 Å to 3.1 Å and local resolution peaks were improved from 3.2 Å to 2.3 Å (Table 1). By combining the improved cryo-EM map with ModelAngelo, a newly developed graph neural network-based approach for automated model building (22), we were able to assign residues to a previously unbuilt region of the PDE6γ subunit and present a more complete structural model of the PDE6 holoenzyme. Strong cryo-EM density for residues Pro55 to Met57 allowed for the identi cation of a new hydrogen bonding network between the glycine-rich region of PDE6γ (residues 55–62) and the dimerization interface of the adjacent PDE6 catalytic subunit (Fig. 2*B*). PDE6γ residues Phe50, Asp52, Pro55, and Thr62 form hydrogen bonds with PDEβ residues Glu249, Arg255, His258, and Asp252,

Table
Cryo-EM data collection re nement and validation statistics

Sample	Apo-PDE6 EMD-42208) PDB 8UFI)	PDE6-udena l EMD-42220) PDB 8UGB)	PDE6-cGMP EMD-42234) PDB 8UGS)	PDE6-IBMX EMD-42358) PDB 8ULG)
Data collection and processing				
Magni cation	79,000	63,000	63,000	63,000
Voltage (kV)	200	200	200	200
Electron exposure (e /Å^2)	50	50	50	50
Defocus range (μm)	1.2 to 2.4	1.4 to 2.0	1.4 to 2.0	1.0 to 2.6
Physical pixel size (Å)	1.034	1.31	1.31	1.34
Symmetry imposed	C1	C1	C1	C1
Initial particle images (no.)	1,300,728	4,731,596	3,578,031	4,950,970
Final particle images (no.)	457,179	2,050,380	788,557	863,564
Map resolution (Å)	3.1	3.0	3.2	3.2
FSC threshold	0.143	0.143	0.143	0.143
Map resolution range (Å)	2.3–8.8	2.7–8.0	2.8–8.0	2.9–8.0
Re nement				
Initial model used	ModelAngelo	ModelAngelo	ModelAngelo	ModelAngelo
Model resolution (Å)	3.05	2.90	3.01	3.00
FSC threshold	0.143	0.143	0.143	0.143
Map sharpening *B* factor (Å^2)	50	20	20	100
Model composition				
Nonhydrogen atoms	14,157	13,726	13,961	14,635
Protein residues	1734	1669	1701	1789
Ligands	6	8	8	8
B factors (Å^2)				
Protein	132.29	103.80	96.21	101.29
Ligand	135.64	108.68	95.71	90.13
RMSD				
Bond lengths (Å)	0.004	0.004	0.002	0.002
Bond angles (°)	0.533	0.629	0.528	0.536
Validation				
MolProbity score	1.59	1.92	1.52	1.55
Clash score	7	7	5	5
Poor rotamers ( )	1.5	1.4	2.0	1.8
Ramachandran plot				
Favored ( )	96.27	94.52	96.63	96.29
Allowed ( )	3.49	5.18	3.32	3.66
Disallowed ( )	0.30	0.30	0.06	0.06

Abbreviation: FSC, Fourier shell correlation.

respectively, through interactions both between side chains and with the polypeptide backbone.

Taking advantage of recent advances in analyzing continuous conformational motion in cryo-EM data, we performed 3DVA to investigate PDE6 conformational dynamics. 3DVA is a method implemented in cryoSPARC for tting 3D linear subspace models to single particle cryo-EM data and can be used to explore conformational flexibility and subunit occupancy (23). The mask and particles from the consensus 3.1 Å re nement were used as an input to 3DVA with three components and the results were ltered to 6 Å resolution for visualization (Fig. S2, *A* and *B*). Notably, despite its intrinsically disordered nature, PDE6γ adopts a largely stable conformation and remains tightly associated with the PDE6 β subunit core across all variability components (Figs. 2*C* and S3). For the PDE6 heterotetramer, the rst variability component resolves bending of the PDE6 GAF domains toward the PDE6β catalytic core, which is associated with destabilization of the ponytail motif" (Fig. S2*C*). The second variability component resolves twisting of the GAF domains around the dimerization helices (*i e* , formed by the two large PDE6 and PDE6β catalytic subunits), which is accommodated by movement of the

Table 2
Cryo-EM data collection re nement and validation statistics for anisotropic maps without a deposited atomic model

Sample	PDE6 bound to two chimera G $_T$* without a stabilizing antibody EMD-42238)	PDE6 bound to one retinal G $_T$ GTPγS EMD-42235)	PDE6 bound to two retinal G $_T$ GTPγS EMD-42237)
Data collection and processing			
Magni cation	79,000	63,000	63,000
Voltage (kV)	200	200	200
Electron exposure (e /Å^2)	50	50	50
Defocus range (μm)	1.2 to 2.4	1.0 to 2.6	1.0 to 2.6
Physical pixel size (Å)	1.034	1.34	1.34
Symmetry imposed	C1	C1	C1
Initial particle images (no.)	552,156	4,950,970	4,950,970
Final particle images (no.)	198,342	59,607	42,479
Map resolution (Å)	4.44	4.15	4.24
FSC threshold	0.143	0.143	0.143

Abbreviation: FSC, Fourier shell correlation.

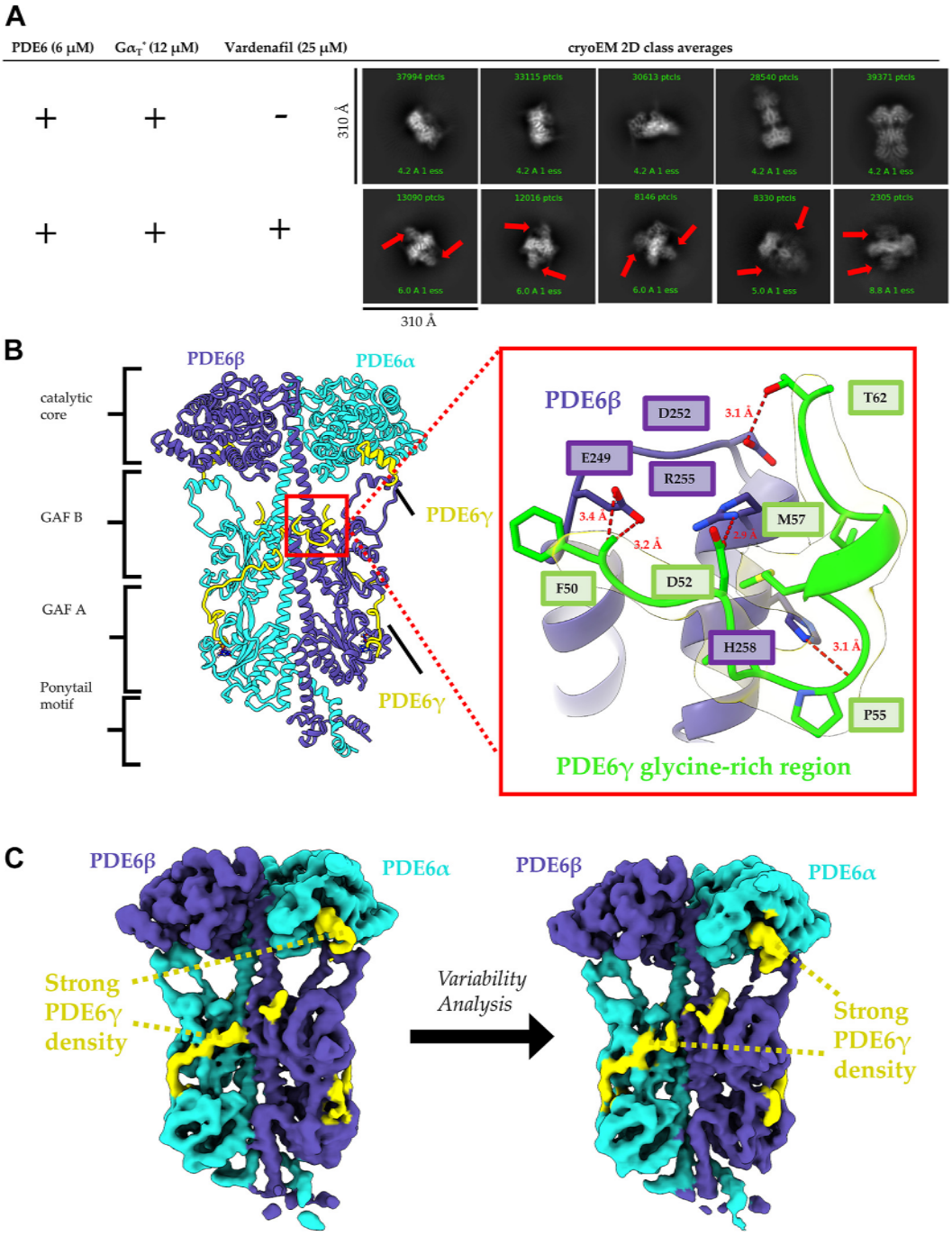

Figure 2. The glycine-rich region of PDE6γ binds near the PDE6 dimerization interface. *A*, comparison of 2D classes of the G $_T$* PDE6 complex, with and without vardena l treatment. In the presence of vardena l, the G $_T$* PDE6 complex forms at a 2:1 stoichiometric ratio and does not readily form in its absence. The G $_T$* subunit is indicated by the red arrows. *B*, the improved cryo-EM structure of the PDE6 heterotetramer. The PDE6 (*cyan*), PDE6β (*purple*), and PDE6γ (*yellow*) are denoted and the domains of the PDE6 holoenzyme are labeled. The hydrogen bonding network between the PDE6γ glycine-rich region (*green*) and PDE6β (*purple*) is shown in the insert (*red*) with the cryo-EM density (*yellow*). *C*, 3DVA shows that PDE6γ remains tightly associated with the PDE6 and PDE6β across all variability components (also see Fig. S3). 3DVA, 3D variability analysis; PDE, phosphodiesterase.

catalytic cores toward the GAF domains, resulting in a slight compaction of the enzyme (Fig. S2*C*). The third variability component resolves bending of the GAF domains away from the catalytic cores of both PDE6 and PDE6β subunits on one face, which is coordinated with movement of the GAF domains toward the catalytic cores of the other face (Fig. S2*C*).

We then used cryo-EM to solve a high-resolution structure of PDE6 bound to udena l (Table 1). The resulting cryo-EM map was re ned to 2.9 Å resolution and the initial atomic model was generated using ModelAngelo (Fig. 3). The catalytic cores of the apo- and udena l-bound PDE6 are remarkably similar, with an overall RMSD of 0.3 Å when aligned by the PDE6 catalytic site; however, there is minimal cryo-EM map density for the C termini of the PDE6γ subunits, which bind near the PDE6 active sites in apo-PDE6, as well as a weakened density for the glycine-rich region of PDE6γ (Fig. 3*A*). The